Received: 2 June 2020 | Accepted: 25 October 2020

DOI: 10.1002/sctm.20-0234

TISSUE ENGINEERING AND REGENERATIVE MEDICINE

STEM CELLS TRANSLATIONAL MEDICINE

Comparison of concentrated fresh mononuclear cells and cultured mesenchymal stem cells from bone marrow for bone regeneration

Fengzhou Du[1,2] | Qian Wang[1] | Long Ouyang[1] | Huanhuan Wu[1] | Zhigang Yang[1] | Xin Fu[1] | Xia Liu[1] | Li Yan[1] | Yilin Cao[1] | Ran Xiao[1]

[1]Research Center of Plastic Surgery Hospital, Chinese Academy of Medical Sciences & Peking Union Medical College, Beijing, People's Republic of China

[2]Department of Plastic and Reconstructive Surgery, Peking Union Medical College Hospital, Chinese Academy of Medical Sciences and Peking Union Medical College, Beijing, People's Republic of China

Correspondence
Ran Xiao, DDS, PhD, Professor and Director, Chinese Academy of Medical Sciences & Peking Union Medical College, 33 Ba-Da-Chu Road, Beijing 100144, People's Republic of China.
Email: xiaoran@psh.pumc.edu.cn

Yilin Cao, MD, PhD, Professor, Chinese Academy of Medical Sciences & Peking Union Medical College, 33 Ba-Da-Chu Road, Beijing 100144, People's Republic of China.
Email: yilincaoplastic@163.com

Funding information
Non-profit Central Research Institute Fund of Chinese Academy of Medical Sciences, Grant/Award Number: 2018PT32015; Beijing Municipal Science & Technology Commission, Grant/Award Numbers: D090800046609003, Z181100001718188

Abstract

Autologous bone marrow mononuclear cell (BMMNC) transplantation has been widely studied in recent years. The fresh cell cocktail in BMMNCs, without going through the in vitro culture process, helps to establish a stable microenvironment for osteogenesis, and each cell type may play a unique role in bone regeneration. Our study compared the efficacy of concentrated fresh BMMNCs and cultured bone marrow-derived mesenchymal stem cells (BMSCs) in Beagle dogs for the first time. Fifteen-millimeter segmental bone defects were created in the animals' tibia bones. In BMMNCs group, the defects were repaired with concentrated fresh BMMNCs combined with β-TCP (n = 5); in cultured BMSC group, with in vitro cultured and osteo-induced BMSCs combined with β-TCP (n = 5); in scaffold-only group, with a β-TCP graft alone (n = 5); and in blank group, nothing was grafted (n = 3). The healing process was monitored by X-rays and single photon emission computed tomography. The animals were sacrificed 12 months after surgery and their tibias were harvested and analyzed by microcomputed tomography and hard tissue histology. Moreover, the microstructure, chemical components, and microbiomechanical properties of the regenerated bone tissue were explored by multiphoton microscopy, Raman spectroscopy and nanoindentation. The results showed that BMMNCs group promoted much more bone regeneration than cultured BMSC group. The grafts in BMMNCs group were better mineralized, and they had collagen arrangement and microbiomechanical properties similar to the contralateral native tibia bone. These results indicate that concentrated fresh bone marrow mononuclear cells may be superior to in vitro expanded stem cells in segmental bone defect repair.

KEYWORDS

bone marrow-derived mesenchymal stem cells, bone regeneration, concentrated bone marrow mononuclear cells, β-TCP

1 | INTRODUCTION

Bone marrow-derived mesenchymal stem cells (BMSCs) have significant bone repair and regeneration potential. However, in vitro culture of BMSC require a long time, higher manufacturing cost, especially good manufacturing practice facility and have the risk of contamination.[1] In that, these factors make the cells requiring in vitro amplification unsuitable for clinical use. Relative to BMSCs, bone marrow mononuclear cells (BMMNCs) consist of a number of cell types, including mesenchymal stem cells, endothelial stem cells, hematopoietic stem cells, and lymphocytes,[2,3] with BMSCs being a subpopulation of them. BMSCs are one of them. BMMNCs can be directly applied without going through the in vitro culture process, which can greatly save time and treatment costs, and avoid the differentiation and migration ability decline caused by in vitro culture and expansion, as well as contamination risk and other uncertain factors.

There are mainly two methods to increase the number of BMSCs: concentrated fresh bone marrow mononuclear cells or culture of BMSCs in vitro.[4-11] Compared with certain purified cells in bone marrow, BMMNCs secrete various growth factors and cytokines that promote tissue regeneration and repair, providing a microenvironment for interaction, differentiation, and induction between cells.[12,13] BMMNCs has been reported to have the potential to promote angiogenesis and bone regeneration.[14] BMMNCs have been used for nonunion transplantation, but are rarely used for the repair of large segmental bone defects.[6] In a recent study, BMMNCs were used to treat alveolar bone clefts.[15] The easy accessibility and bone regeneration ability make them good candidates for bone repair. TCP was chosen as the carrier in this study. Granular TCP has three-dimensional porous structure, which is conducive to cell adhesion and migration to the internal scaffold, and at the same time promotes the formation of new bone, which may accelerates the degradation rate of scaffolds.[16]

However, there have been no reports on the difference in the efficacy of BMMSCs and BMMNCs from bone marrow on large segmental bone defect. To study the advantages of BMMNCs in bone defect repair, this study compared and analyzed the difference in the efficacy of BMMSCs and BMMNCs combined with β-TCP transplantation in the treatment of canine critical-size segmental bone defect. Furthermore, new technologies such as multiphoton microscopy and Raman spectroscopy were adopted to explore the microstructure and chemical components of the new bone tissue.

Significance statement

The study compared the efficacy of concentrated fresh bone marrow mononuclear cells (BMMNCs) and cultured bone marrow-derived mesenchymal stem cells (BMSCs) in segmental bone defect of Beagle dogs. The results showed that concentrated fresh BMMNCs promoted much more bone regeneration than cultured BMSCs. The grafts in BMMNCs group were better mineralized, and they had similar collagen arrangement and microbiomechanical properties with the native bone. We confirm that using autologous BMMNCs combined with Î²-TCP could be another treatment option for large-scale bone defects. The therapeutic method is promising and encourages further mechanism research.

2 | MATERIALS AND METHODS

2.1 | Animals and ethics

The animal experiments were approved by the Institutional Animal Care and Use Committee of the Plastic Surgery Hospital, PUMC. All experiments were performed in accordance with local and institutional guidelines. Eighteen Beagle dogs (male, average weight 11 kg, age 14-17 months) were involved in this study. All animals were separated in a conventional environment at the Experimental Animal Center of Plastic Surgery Hospital, PUMC. The animals can drink water freely and were fed two times a day with standard canine diet (GB14924.7-2001). A team consists of anesthetist, veterinarian, and nurse managed the drug use during the operation. All animals were closely monitored by the researcher and animal care staff throughout the day. Twelve months after operation, the animals were sacrificed.

2.2 | Graft preparation

Bone marrow aspirates (BMAs) were harvested from the iliac bone of Beagle dogs. The volume of the BMAs was 15 mL for both groups. In order to avoid collecting peripheral blood, we aspirate in four different areas around the ilium.[5,17] Mononuclear cells were isolated from the aspirate by Ficoll density gradient centrifugation (GE Healthcare Bio-Sciences, Pittsburgh, Pennsylvania). In the BMMNCs group, the cells were washed and resuspended with autologous plasma to a final volume of 0.5 mL with an average total nucleated cell concentration of $33.0 \pm 8.8 \times 10^6$/mL. The fresh BMMNCs suspension was added to the pre-wetted β-TCP scaffold during the animal surgery. The BMMNCs prepare was described before.[18] Samples of BMMNCs suspension, the peripheral blood plasma (PBP) and the whole BMA were collected for cytokine assays according to the manufacturer's directions using Quantibody@ Canine Cytokine Array kits (Ray Biotech, Inc, Peachtree Corners, Georgia).

In the BMSC group, the cells were cultured in 20 mL of Dulbecco's-modified Eagle's Medium-Low Glucose (DMEM-LG, Gibco) and incubated at 37°C and 5% CO_2. After 2 days, the non-adherent cells were removed by changing the culture medium. The cells were treated with trypsin when grown to 80% confluence and diluted to 1:3 per passage for further expansion. Cells at passage 2 were used in experiments. The cells were harvested and seeded onto the β-TCP scaffold at a concentration of 20×10^6 cells/mL (approximately 10×10^6 cells per scaffold). Our previous study demonstrated that 76% to 89% of BMSCs adhered onto β-TCP scaffold after 24 hours.[19] The BMSCs/scaffold constructs were kept in culture in an osteogenic medium (DMEM supplemented with 10% fetal bovine

serum (FBS), ascorbic acid-phosphate 50 μg/mL, dexamethasone 10 nM, and β-glycerophosphate sodium 10 mM) for 2 weeks. The constructs were washed twice with PBS (PBS, HyClone) immediate before surgery. The osteogenic differentiation of BMSCs was confirmed by positive results of alizarin red staining (Supplementary Figure 1).

The microstructured β-TCP scaffold (Bio-lu Bioceramics, Bio-lu Biomaterials Co. Ltd, Shanghai, China) was cylindrical and had a diameter of 12 mm and a length of 17 mm. A central tube (diameter: 3 mm) ran along the long axis. The porosity of the scaffold was 75% ± 10%. The diameter of the macropores was 500 ± 150 μm, and the diameter of the interconnected pores was 150 ± 50 μm.

2.3 | Segmental bone defect model

Under general anesthesia, the animals underwent surgery to remove a 15 mm segment of the mid-diaphyseal tibia. The remaining bone was stabilized with a titanium plate. Three screws were inserted on each side of the defect. The defects were randomly divided into four groups: BMMNCs group, where the defects were repaired with fresh BMMNCs combined with β-TCP (n = 5); BMSC group, with in vitro cultured and osteo-induced BMSCs combined with β-TCP (n = 5); scaffold-only group, with a β-TCP graft alone (n = 5); and blank group, without any graft (n = 3). Animals were allowed unrestricted weight bearing after surgery. The titanium plates were removed at 6 months if osteotomy lines were invisible, or at the 12-month of observation. X-ray was performed at 2 weeks, 3 months, 6 months, and 12 months after surgery to monitor the bone healing process.

2.4 | Single photon emission computed tomography

Single photon emission computed tomography (SPECT) was used to evaluate bone growth and vascularization of the grafts in vivo. The SPECT/CT system (Infinia VC Hawkeye4, GE) equipped with a spiral CT. ^{99m}Tc methylene diphosphonate (MDP) was injected intravenous at a dose of 185 MBq. The hybrid images of SPECT and CT were obtained 4 hours after injection. All images were reviewed by two experienced nuclear medicine physicians. The region of interest (ROI) was selected manually. The uptake ratios of ^{99m}Tc MDP (T/NT) were calculated.

2.5 | Micro-CT

A micro-CT system (μCT-1076, Skyscan, Belgium) was used to visualize the newly formed mineralized tissue of the tibial specimens. The specimens were scanned at a voltage of 70 kV, a current of 140 μA, and a voxel size of 19 μm. Only the defect areas were selected as ROI. Lower grey threshold of 70 and upper grey threshold of 120 were chosen to include the mineralized tissue and exclude scaffold and soft tissue. Within ROI, the bone tissue mineral density (TMD), regenerated bone volume (BV), tissue volume (TV), and bone volume fraction (bone volume/total volume, BV/TV) were calculated by CTAn program (Bruker, Skyscan microCT, Belgium).

2.6 | Histological examination

The specimens were dehydrated by gradient alcohols from 70% to 100%. The specimens were then embedded in polymethyl methacrylate (PMMA). The embedded tissue was cut into slices using a saw microtome (300CP, EXAKT, Germany). The thickness of the slices was 200 μm. The slices include transverse sections perpendicular to the long axis from the midshaft, and also vertical sections parallel to the long axis that could show both the graft and the interface between the graft and the native bone. The slices were polished and sent for multiphoton microscopy, Raman spectroscopy, and nanoindentation. After that, the slices were further ground to 40 μm with an EXAKT 400 grinding system and then stained with methylene blue-acid fuchsine stain[20] and modified Masson-Goldner trichrome stain.[21] Methylene blue-acid fuchsine stain provides remarkable contrast between bone and other tissues. The bone is dyed bright pink, and the soft tissue is dyed blue purple. Masson-Goldner trichrome stained mature bone matrix blue, immature new bone matrix red, osteoid, and soft tissue orange.

2.7 | Multiphoton microscopy

Multimodal multiphoton microscopy was used to further investigate the microstructure of the regenerated bone tissue. Thick, unstained transverse sections from the BMMNCs and BMSCs groups were examined with an Olympus Multiphoton Laser Scanning Microscope (FV1000, Olympus, Japan). Both second harmonic generation (SHG) and the endogenous two-photon excitation fluorescence (TPEF) were excited using a 780 nm Mai Tai laser. SHG provided contrast specifically for collagen.[22,23] TPEF was used to image the endogenous fluorophores (mainly elastin, collagen, and flavoproteins within the cells).[24-26] The light was focused onto a section with a ×25, 1.05 numerical aperture water objective. The SHG signals were acquired with a BP filter at 390 nm. The TPEF signals were acquired at 500 nm.

2.8 | Raman spectroscopy

The composition of the graft, autologous bone, and the scaffold was characterized by Raman spectroscopy performed with a Raman microscope (LabRAM HR Evolution, HORIBA Scientific, Japan). The spectra were collected from polished specimen surfaces using a 532-nm laser focused through a ×50, 0.75 numerical aperture air objectives. The spectra were taken at eight points along a line drawn from the center to the outer border of osteon in five randomly chosen osteons. The Raman spectra were baseline corrected before analysis. The mineral/matrix ratio was expressed as the phosphate (961 cm^{-1}) to the CH_2 side-chains band ratio (1450/cm), which indicated the degree of mineralization.[27,28] Carbonate substitution was measured by the

carbonate to phosphate ratio (1070/961/cm), which varied with the bone architecture and the mineral crystallinity.[29,30] Carbonate to amide I ratios (1070/1665/cm) indicated bone remodeling.[31,32]

2.9 | Nanoindentation

A computer-controlled nanoindenter system (Nanoindenter XP, MTS) was used to evaluate the micromechanical properties of the regenerated bone and autologous bone. The displacement resolution was 0.01 nm, and load resolution was 50 nN. During indentation, the indenter was advanced to 220 nm at a speed of 10 nm/s and held for 10 seconds at the peak load. For each specimen, the test sites were selected similarly to those for Raman spectroscopy. Thirty points were randomly selected for nanoindentation. The elastic modulus (E) and contact hardness (H) were calculated from the load-displacement curves using the Oliver-Pharr method.[33]

2.10 | Statistical analysis

Statistical analysis was performed with Student's *t* test (SPSS 17.0, SPSS Inc) All values are presented as mean ± SD. Values of $P < .05$ were considered as statistically significant.

3 | RESULTS

3.1 | Radiographic examination of bone healing within 12 months

To dynamically observe the graft, the animals were examined with x-rays at 14 days, 3, 6, and 12 months postsurgery. For the blank group, none of the defects formed a bone union at 6 months, which indicated that this defect model was a critical size defect (Supplementary Figure 2A,B). Bone bridging of the defect was evident in four of five animals in the BMMNCs group at 3 months after surgery (Figure 1B). The internal fixation was removed at 6 months, and no refractures were observed (Figure 1C). Twelve months after surgery, the bone loss caused by internal fixation disappeared. Signs of remodeling such as the absorption of callus, the increased density of the cortical bone, and the formation of a bone marrow cavity were evident (Figure 1D). In the BMSC group, the osteotomy lines were still radiolucent 6 months after surgery, which led to the inability to remove the titanium plate (Figure 1E-G). Twelve months after surgery, the osteotomy line was partially radiolucent in three of five animals (Figure 1H). In the scaffold-only group, all grafts underwent obvious resorption at 3 months, and the grafts were completely lost at 6 months (Supplementary Figure 2C,D). Eventually, no bony bridge was observed in this group. The x-ray results for the BMMNCs and BMSCs group at each time point were evaluated through a scoring system reported by Yang's group (Supplementary Table 1).[34] The radiographic grading score of both groups showed a time-dependent increase. However, the result indicated that the average score of the BMMNCs group was significantly increased relative to the BMSC group at 3 months (9.6 vs 6.4), 6 months (15.8 vs 9.4), and 12 months (20.2 vs 12.6).

Single photon emission computed tomography/computed tomography (SPECT/CT) was used to detect angiogenesis and the viability of the bone graft at 12 months postoperatively in the BMMNCs and BMSCs groups. Both groups showed obvious radioactivity at the graft area (Figure 1I-L). In the BMMNCs group, the average uptake ratio of ^{99m}Tc-MDP (target to nontarget ratio, T/NT) was 7.35, whereas the ratio in the BMSCs group was 3.91 (Figure 1M). The difference was significant.

3.2 | Gross observation and micro-CT analysis

The tibias were collected and inspected after sacrifice at 12 months postoperatively. In the BMMNCs group, gross observation revealed that the graft area was slightly enlarged, and the contour was smooth (Figure 2A). The bone graft and native bone could not be distinguished. Large amounts of bone formation were observed both outside the scaffold and inside the macro pores of the scaffold. The peripheral bone appeared to be cortical bone, and the central bone appeared similar to cancellous bone (Figure 2B). The scaffolds in the BMSC group were visible, and only a little bone was formed around the scaffold (Figure 2D). Nevertheless, a cross section showed considerable bone formation inside the scaffold (Figure 2E).

The specimens were subjected to a micro-CT examination (Figure 2C,F) for additional quantitative analysis. Animated micro-CT scans of a representative sample of the BMMNCs and BMSC groups from proximal to distal are shown in Supplementary Movies 1 and 2. The average BV of the BMMNCs group was 1231.38 mm^3, and the average bone volume fraction (BV/TV) was 65.14%, which were significantly higher than BMSC group that had an average BV of 755.65 mm^3 and an average BV/TV of 41.29% (Figure 2G,H). However, the average TMD in the BMMNCs group (690.4 mg/cm^3) was not significantly different from the average TMD in the BMSC group (668.6 mg/cm^3) (Figure 2I).

3.3 | Histological examination

The morphology of the regenerated bone tissue was further investigated by hard tissue histology. The nondecalcified sections were stained with methylene blue/acid fuchsine and modified Masson-Goldner trichrome stain. Consistent with the micro-CT results, the cross section in the BMMNCs group showed no obvious boundaries at the interface of regenerated bone and native tibia bone (Figure 3A). The bone tissue inside the macropores was well mineralized. The regenerated tissue was rich in blood vessels that were located at the Haversian canals and the walls of the macropores (Figure 3B,G). Under higher power, the Haversian system was well-defined, with five to seven layers of lamellae surrounding it. Osteocytes were embedded in the lacunae between the

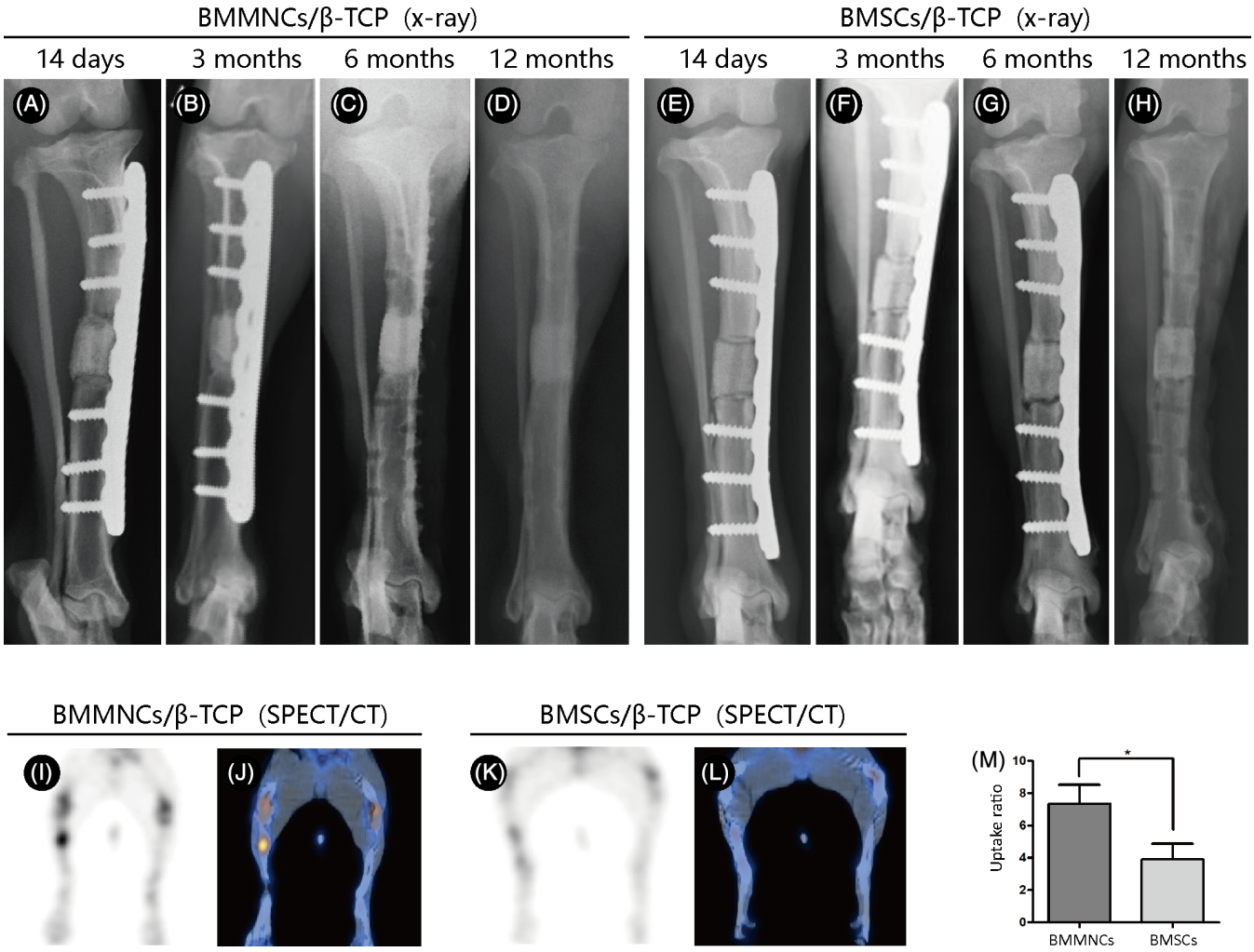

FIGURE 1 Bone marrow mononuclear cells (BMMNCs)/β-TCP repaired segmental defects in Beagle dogs. A-D, Representative X-ray images showing the healing process of a subject in the BMMNC group (n = 5) at 14 days (A), 3 months (B), 6 months (C), and 12 months (D). E-H, Representative X-ray images of a subject in the bone marrow-derived mesenchymal stem cell (BMSC) group (n = 5) at 14 days (E), 3 months (F), 6 months (G), and 12 months (H). I-L, SPECT and SPECT/CT fusion images showing the concentration in the graft area in the BMMNC group (I, J) and the BMSC group (K, L). M, Comparison of the uptake ratio in the SPECT of the two groups (*t* test)

lamellae (Figure 3H). The osteons in the bone formed outside of the scaffold were actively forming new lamellae, which was characterized by hypomineralized tissue at the center (Figure 3I,J). In the BMSC group, the regenerated bone was inside the scaffold but near the surface and had obvious interfaces with the native tibia cortical bones (Figure 3K,P). The pores at the center of the scaffold were filled with osteoid and fibrous tissue (Figure 3S,T). The degree of mineralization in BMSC group was lower than that in the BMMNCs group.

3.4 | Microstructure analysis of regenerated bone tissue by multiphoton microscopy

High-resolution SHG images showed the organization of the collagen network. The TPEF images showed contrast gained from abundant endogenous fluorophores of the cells and the matrix of bone tissue. Notably, the blood vessels revealed strong TPEF signals but no SHG signals. Within the macropores of the BMMNCs group, the collagen fibers were either arranged concentrically around the vascular tissue or aligned in layers (Figure 4B). Osteocytes were observed between the lamellae (Figure 4A). More lacunae but fewer osteocytes were observed in the TPEF images outside of the scaffold (Figure 4D), and the collagen fibers were better organized (Figure 4E) and quite similar to those in native cortical bone (Figure 4J-L). However, the collagen fibers in the BMSC group were disorganized and had a lower density. The collagen network was concentrated on the walls of the macro pores (Figure 4G-I).

3.5 | Bone composition and biomechanical analyses

The typical Raman spectra of specimens from the BMMNCs group, BMSC group, the autotibia, and the β-TCP scaffold are presented in

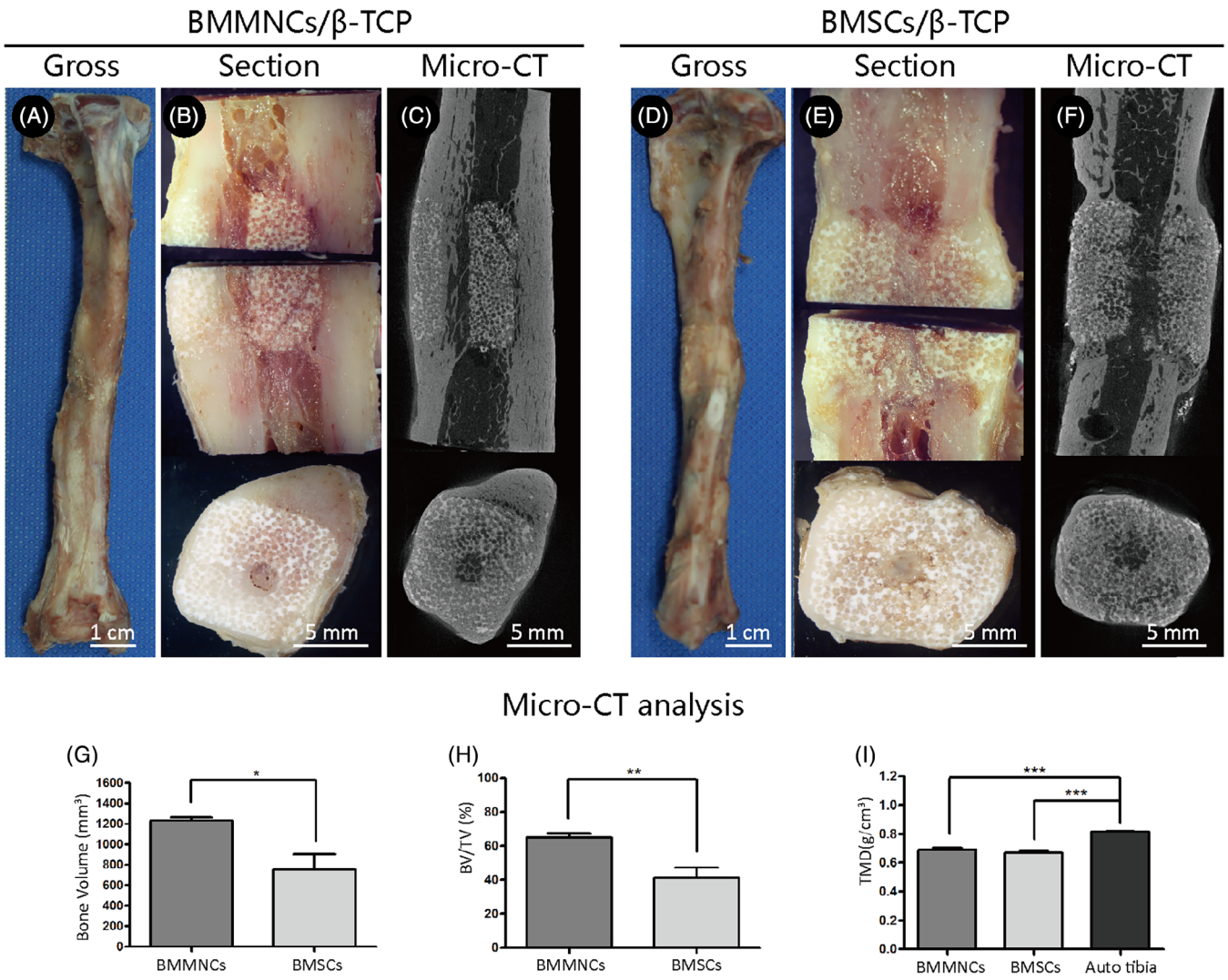

FIGURE 2 Gross observations and micro-CT analysis showing massive bone regeneration after bone marrow mononuclear cells (BMMNCs)/β-TCP grafting. A-F, Gross view, section view, and micro-CT images of the tibia at 12 months after surgery in the BMMNC (A-C) and the bone marrow-derived mesenchymal stem cell (BMSC) (D-F) groups. The section views are displayed in proximal, distal and transverse segments. G-I, Micro-CT analysis results. BV (G) and BV/TV (H) were significantly higher in the BMMNC group. TMD (I) in the BMMNC and BMSC groups were not significantly different but were lower than in the contralateral autotibia (*t* test)

Figure 5A. The autologous tibial bone, BMMNCs, and BMSC specimens showed similar peak positions, but the intensities at certain Raman shifts were different. Most of the Raman bands could be assigned to bone mineral and matrix collagen.

The degree of bone mineralization could be expressed by the mineral to matrix ratio (961/1451/cm). The ratio in BMMNCs group, although lower than the autologous tibial bone, is a significantly increased compared with that in the BMSC group (Figure 5B). The carbonate to phosphate ratio (1070/961/cm), a parameter that indicates carbonate substitution, was significantly increased in both BMMNCs and BMSC group compared to the autologous tibial bone (Figure 5C). Bone remodeling was indicated by a carbonate to amide I ratio (1070/1665/cm). The BMMNCs group showed significantly greater tissue remodeling than the other groups (Figure 5D). None of the above indicators varied significantly across the osteons.

Eight indentations were measured across the radii of osteons for micromechanical property evaluation. The indentation modulus and the hardness were calculated from a nanoindentation load-displacement curve (Figure 5F-H). In the BMMNCs group, the average indentation modulus was 4.68 GPa, and the average hardness was 0.64 GPa, which was close to that of the autotibia and significantly increased relative to the BMSC group (Figure 5I,J). The indentation modulus and hardness did not vary across the osteons.

3.6 | Analysis of cytokines in the BMMNCs suspension

The cytokines in the BMMNCs suspension were analyzed and compared with those in the PBP and in the BMA (Figure 6). The results showed that the BMMNCs suspension had an higher IL-8

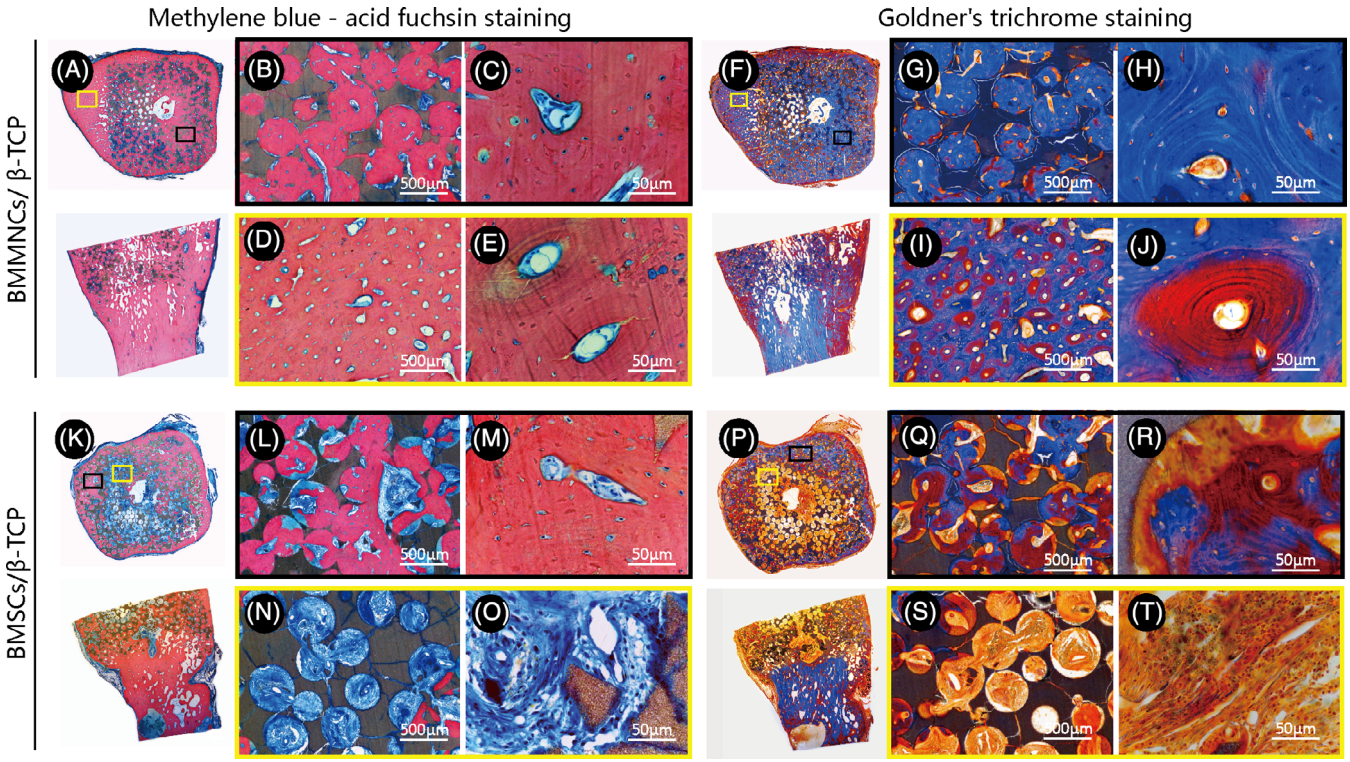

FIGURE 3 Histology of the grafts in the bone marrow mononuclear cell (BMMNC) and bone marrow-derived mesenchymal stem cell (BMSC) groups at 12 months after surgery. A-E, Methylene blue-acid fuchsine staining in the BMMNCs/β-TCP treated animals. Cross and longitudinal sections show newly formed bone tissue (bright pink) and an undegraded scaffold (A). The macropores of the scaffold were filled with bone tissue (B). Blood vessels were located in the Haversian canals (C) and on the walls of the macropores. The Harversian system could also be visualized in the regenerated bone tissue around the scaffold (D, E). F-J, Modified Goldner's trichrome staining of the graft from the BMMNC group. Newly formed bone around the scaffold included hypomineralized bone tissue (red) (F), which was located at the center of the osteons (I, J). The bone tissue in the macro pores was well-mineralized (blue) (G), and the osteocytes were well-defined between the lamellae (H). K-T, Histology of the animals in the BMSC group. Newly formed bone tissue was visualized inside the scaffold (K-M), but the pores near the center of the graft were filled with soft tissues (blue) (N, O). There was a clear interface with the native cortical bone (P). The regenerated bone tissue was not fully mineralized in most areas (orange) (S, T)

level compared to the PBP and BMA. BMMNCs suspension and BMA had a lower concentration of the receptor for advanced glycation end products (RAGE) and stem cell factor (SCF) compared to PBP.

4 | DISCUSSION

The current 12-month evaluation of the long-term effects of bone grafts compared the efficacy of concentrated fresh BMMNCs and cultured BMSCs, in repairing critical size segmental defects of large animals for the first time. The two groups represent different bone regeneration strategies. The cells numbers were about 16.5 ± 4.4 × 10^6 per scaffold in the BMMNCs group and 10 × 10^6 in the BMSCs group. Previously, we described cell viability and distribution of BMSCs on β-TCP scaffold by live/dead staining.[19] However, it is hard to test the cell viability of fresh prepared BMMNCs. Although the two groups were different on cell number and cell types, the volume of the BMAs were identical (15 mL), which indicate the same extent of donor site morbidity.

Our results showed that BMMNCs combined with β-TCP not only induced much more bone regeneration, but also yielded better new bone quality, similar to native bone tissue. Additionally, the newly formed bone callus outside the scaffold was well-integrated with the native bone tissue at the junction, which we believe played an important role in restoring the overall mechanical properties of the tibia. We also observed the signs of bone remodeling in the BMMNCSs/β-TCP graft, such as a smooth contour, osteons that continued to develop in the cortical area, and the resorption of bone at the center of the graft, suggesting the formation of a marrow cavity. The remodeling process in the BMMNCs group resulted in a higher concentration of radioactivity in the SPECT and a higher carbonate to amide I ratio in Raman spectroscopy as well. It should be noted that our study was conducted in young animals. Previous studies indicated that donor age negatively affects proliferation and differentiation capacity of BMSCs from mice[35] and rats[36] in vitro. Therefore, the efficiency of

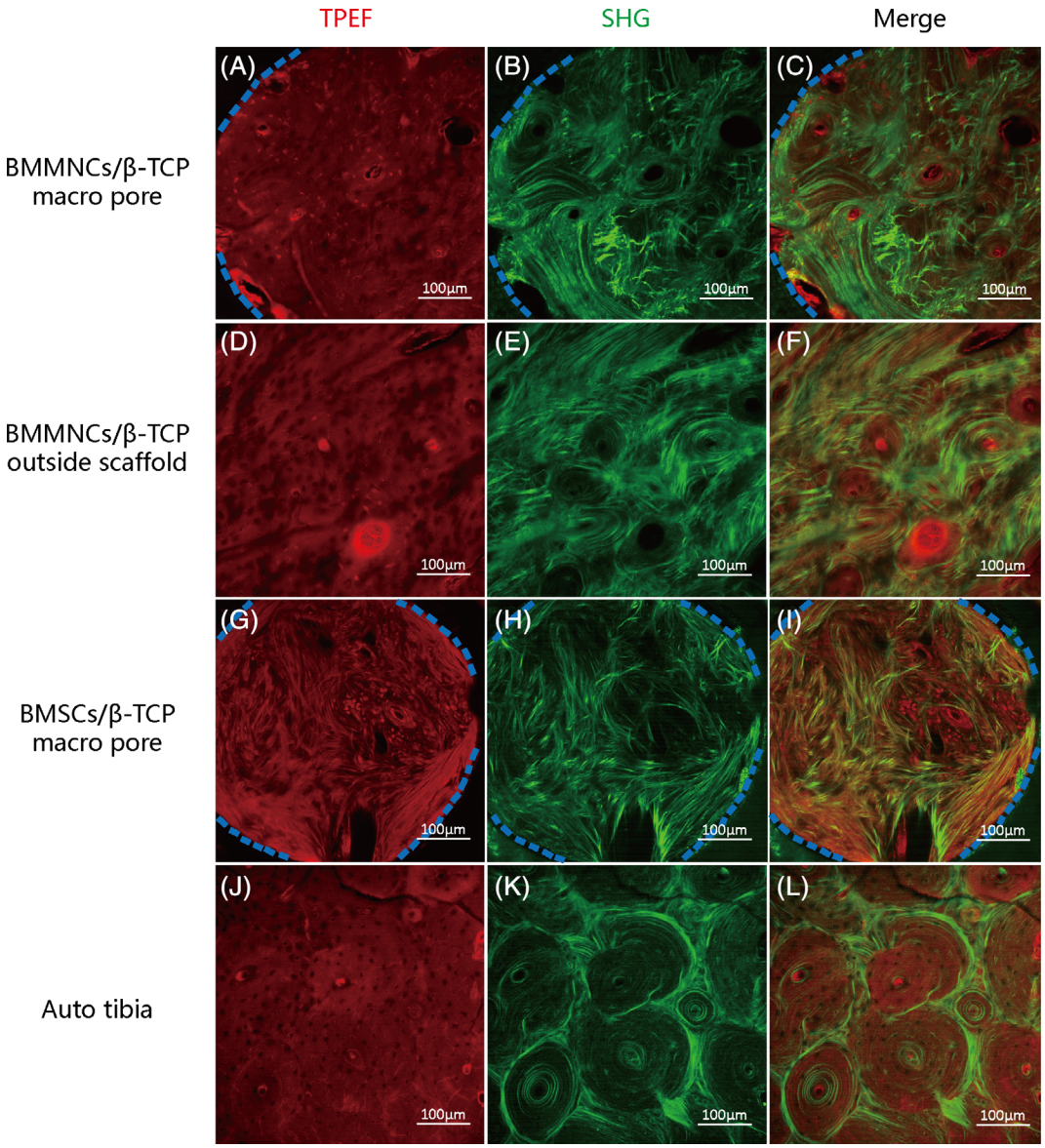

FIGURE 4 Microstructure of the regenerated bone tissue investigated by multiphoton microscopy. A-F, Bone marrow mononuclear cell (BMMNC) group. Two-photon excitation fluorescence (TPEF) image showing the bone matrix, blood vessels, and osteocytes in the macro pores of the scaffold (A). The collagen fibers visualized by SHG were arranged concentrically or aligned in layers near the scaffold (B). The merged image showing blood vessels in the osteons (C). Regenerated bone outside the scaffold showed a deep lacunas (D) and well-organized collagens (E, F). G–I, Bone marrow-derived mesenchymal stem cell (BMSC) group. No lacunas were observed (G), and the collagen fibers were disorganized (H, I). J-L, Contralateral auto tibia. TPEF and SHG images showing well-formed lacunas (J) and osteons (K, L)

BMMNCs and BMSCs for segmental bone defect repairing in adult and elderly subjects needs to be further illustrated.

As a kind of calcium phosphate biomaterial, β-TCP has better degradation rate than hydroxyapatite, and the calcium, phosphorus, and other elements released after the degradation can directly participate in the mineralization of new bone.[37] As an ideal bone repair material, β-TCP with demonstrated osteoconduction and osteoinduction, has been used clinically as a bone void filler.[38,39] Bullin et al seeded BMMNCs onto porous β-tricalcium phosphate scaffold materials for severe maxillary atrophy bone increase.[40]

This study explored the microstructure of the regenerated bone tissue and the bone formation pattern in segmental defects in large animals. By high-resolution TPEF and SHG imaging, the collagen and endogenous fluorophores of the regenerated bone tissue were visualized without staining. In the BMSC group, the collagen density was much lower than in the BMMNCs group, indicating a much earlier stage of osteogenesis. In the BMMNCs group, the collagen formed concentric structures of osteons in the macropores, and the space between the concentric structures were filled with collagen fibers distributed in layers and arranged in a distinct orientation. We speculated that these collagen fibers first formed around the walls of the macropores, then were rearranged after the blood vessels invaded, and new lamellae were deposited around the vessel to form osteons.

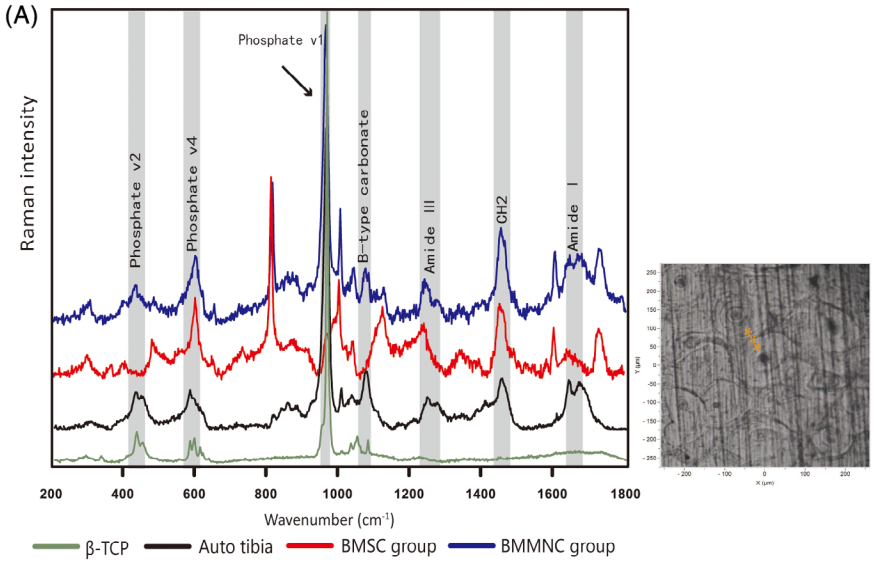

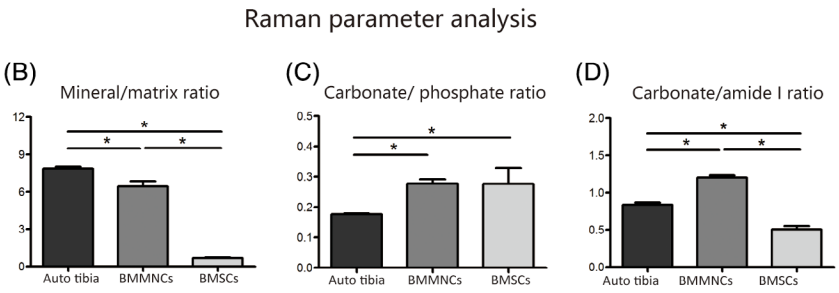

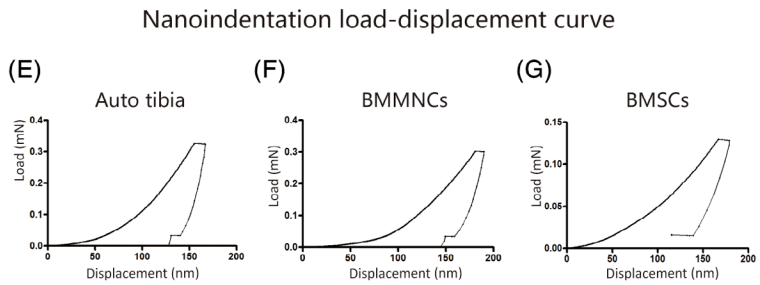

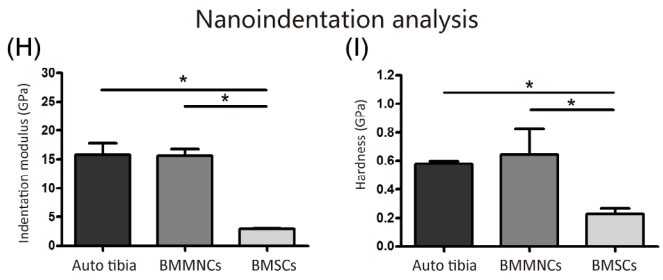

FIGURE 5 Bone compositional and biomechanical analysis. A, Left, typical spectra of bone tissue from the bone marrow mononuclear cell (BMMNC) group, the bone marrow-derived mesenchymal stem cell (BMSC) group, the autotibia and β-TCP scaffold. Right, the test points randomly chosen along the radii of the osteons (B-D) Raman parameter analysis (n = 3 auto tibia, n = 4 BMMNCs, n = 3 BMSCs) of the mineral/matrix ratio (B), carbonate/phosphate ratio (C), and carbonate/amide I ratio (D) (*t* test). F-H, Typical nanoindentation load-displacement curve of specimens from the contralateral autotibia (F), the BMMNC group (G), and the BMSC group (H). I,J, Nanoindentation analysis (n = 3 auto tibia, n = 4 BMMNCs, and n = 3 BMSCs) of the indentation modulus (I) and hardness (J) (*t* test)

The study provided valuable microstructural information on the extent of maturation of the newly formed bone tissue, as indicated by Raman spectroscopy. The average mineral/matrix ratio in the BMMNCs group, approximately 80% of the ratio measured in the contralateral autologous tibial bone, was much higher than in the BMSC group. The mineral/matrix ratio, indicating the amount of mineralization, was the strongest Raman predictor of the mechanical properties of bone.[22,41] The nanoindentation test showed the regenerated bone in the BMMNCs group had an indentation modulus and hardness similar to those of the contralateral tibia. On the other hand, both BMMNCs and BMSC groups showed higher carbonate substitution than the contralateral native tibia bone. This indicated the presence of transitional or immature bone.[42] As mentioned above, the BMMNCs group showed evident remodeling in radiological and histological

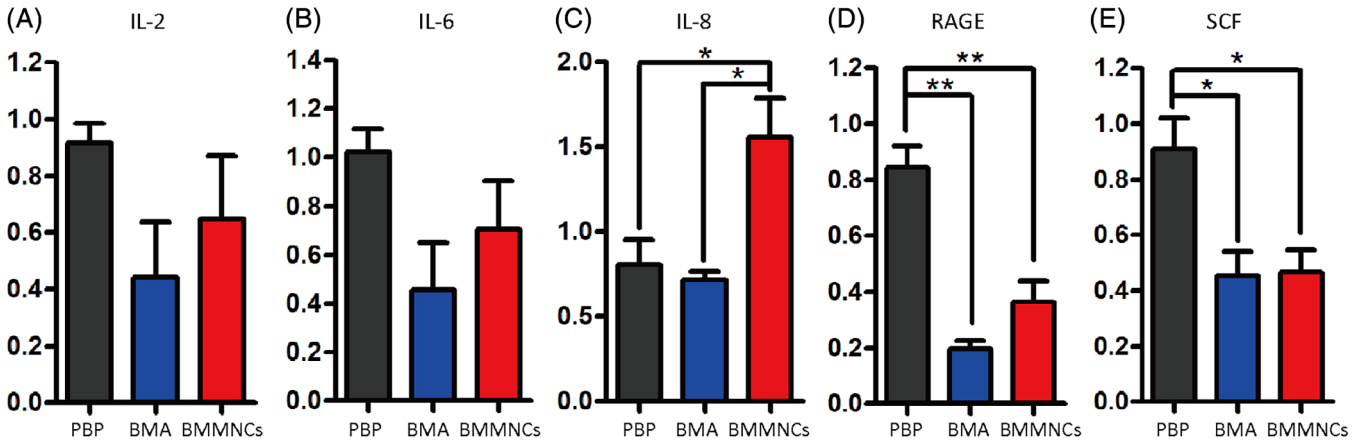

FIGURE 6 Analysis of cytokines in the bone marrow mononuclear cell (BMMNC) suspension. A-E, Relative levels of IL-2 (E), IL-6 (F), IL-8 (G), RAGE (H), and SCF (I) in PBP (n = 3), BMA (n = 3), and BMMNCs (n = 10) of the Beagle dogs (*t* test)

results. In Raman spectroscopy, its intense remodeling was reflected by higher carbonate to amide I ratio.

The concentrated fresh BMMNCs and the in vitro expanded BMSCs had distinctly different components. Here, we did not analyze the function of each component of the BMMNCs in bone regeneration because we believe its effectiveness is a comprehensive result of multiple cell types and cytokines. The cells in BMMNCs suspension include monocytes, lymphocytes, neutrophils, MSCs, hematopoietic stem cells (HSCs), and endothelial progenitor cells (EPCs). This cell cocktail helps to establish a stable microenvironment for osteogenesis, and each component cell type may play a unique role in tissue regeneration. Some studies have indicated that mixed bone marrow-derived cell populations may have a better bone regeneration potential than a population containing a specific cell type.[43]

For example, a recent study demonstrated a crucial role for neutrophils in initiating downstream responses leading to bone regeneration.[44] A lower number of neutrophils resulted in higher IL-6 and IL-10 levels and enhanced macrophage recruitment, which led to impaired bone regeneration. Although the in vitro cultured BMSCs could achieve a very high cell concentration, most of the cells were dead a short time after transplantation.[45,46] Moreover, the differentiation potential and gene expression of BMSCs may be altered during in vitro culture.[47,48] Therefore, the therapeutic effects of BMSCs may be significantly less after in vitro culture.[49] It is well known that autologous BMMNCs improve blood supply because they contain angiogenic factors provided by $CD34^+$ endothelial precursor cells and $CD34^-$ cells.[50] A possible mechanism is that BMMNCs implantation might be useful not only for revascularization, After BMMNCs implantation, osteoblasts and endothelial progenitor cells will differentiate to bone and endothelial cells, finally promoting angiogenesis and leading to bone regeneration.[51]

Ex vivo expansion of BMSCs has been performed using basal culture media plus supplements to provide growth factors, proteins, and enzymes to support cell growth.[52] FBS is the most commonly used to supplement MSC cultures, because it is enriched with growth factors and poor in antibodies. Although MSCs can internalize xenogeneic proteins, which may increase the risk of infection and immunoreaction, over 80% of proposals submitted to FDA for MSC-based products report expansion in FBS.[53] In this study, FBS was also used to expand MSCs in vitro, and it was changed to PBS before the delivery of the construct for animal experimentation. Unlike BMSCs/β-TCP constructs that were washed carefully with phosphate buffer solution to remove heterologous serum before grafting, the BMMNCs/β-TCP graft included autologous plasma from the bone marrow containing various cytokines. Our study demonstrated the BMMNCs suspension had a significantly higher IL-8 level than the PBP or BMA, which was consistent with previous report.[54] It was reported that IL-8 could enhance bone regeneration by recruiting MSCs to the site of the defect.[55] Both the BMMNCs suspension and the whole bone marrow showed a decreased concentration of RAGE and SCF, which are responsible for mediating pro-inflammatory cytokines and can impair the maintenance of MSCs.[56-58] The BMMNCs suspension may protect the graft from an intense inflammatory response after implantation and could recruit more stem cells for bone regeneration.

5 | CONCLUSIONS

The study compared the efficacy of concentrated fresh BMMNCs and cultured BMSCs in segmental bone defect of Beagle dogs. The results showed that concentrated fresh BMMNCs promoted much more bone regeneration than cultured BMSCs. The grafts in BMMNCs group were better mineralized, and they had similar collagen arrangement and microbiomechanical properties with the native bone. We confirm that using autologous BMMNCs combined with β-TCP could be another treatment option for large-scale bone defects. The therapeutic method is promising and encourages further research.

ACKNOWLEDGMENTS

This work was supported by the Beijing Municipal Science & Technology Commission (Z181100001718188, D090800046609003) and the Non-profit Central Research Institute Fund of Chinese Academy of Medical Sciences (2018PT32015).

CONFLICT OF INTEREST

The authors declared no potential conflicts of interests.

AUTHOR CONTRIBUTIONS

F.D.: experiments design, collection and assembly of data, data analysis and interpretation, and manuscript writing. Q.W.: animal surgery. L.O.: manuscript revision. H.W., Z.Y.: collection and assembly of data. X.F., X.L., L.Y.: data analysis and interpretation. R.X., Y.C.: conception and design, final approval of manuscript, and oversaw the collection of results and data interpretation.

DATA AVAILABILITY STATEMENT

All data generated or analyzed during this study are included in this article.

ORCID

Long Ouyang https://orcid.org/0000-0002-2116-320X
Xia Liu https://orcid.org/0000-0003-0832-7772

REFERENCES

1. Wise JK, Alford AI, Goldstein SA, Stegemann JP. Comparison of uncultured marrow mononuclear cells and culture-expanded mesenchymal stem cells in 3D collagen-chitosan microbeads for orthopedic tissue engineering. *Tissue Eng Part A*. 2014;20(1–2):210-224.
2. Lekholm U, Wannfors K, Isaksson S, Adielsson B. Oral implants in combination with bone grafts. A 3-year retrospective multicenter study using the Branemark implant system. *Int J Oral Maxillofac Surg*. 1999;28(3):181-187.
3. Hernigou P, Poignard A, Beaujean F, Rouard H. Percutaneous autologous bone-marrow grafting for nonunions. Influence of the number and concentration of progenitor cells. *J Bone Joint Surg Am*. 2005;87(7):1430-1437.
4. Daltro GC, Fortuna V, de Souza ES, et al. Efficacy of autologous stem cell-based therapy for osteonecrosis of the femoral head in sickle cell disease: a five-year follow-up study. *Stem Cell Res Ther*. 2015;6:110.
5. Lee DH, Ryu KJ, Kim JW, Kang KC, Choi YR. Bone marrow aspirate concentrate and platelet-rich plasma enhanced bone healing in distraction osteogenesis of the tibia. *Clin Orthop Relat Res*. 2014;472(12):3789-3797.
6. Johnson RG. Bone marrow concentrate with allograft equivalent to autograft in lumbar fusions. *Spine*. 2014;39(9):695-700.
7. Rickert D, Vissink A, Slot WJ, Sauerbier S, Meijer HJ, Raghoebar GM. Maxillary sinus floor elevation surgery with BioOss(R) mixed with a bone marrow concentrate or autogenous bone: test of principle on implant survival and clinical performance. *Int J Oral Maxillofac Surg*. 2014;43(2):243-247.
8. Quarto R, Mastrogiacomo M, Cancedda R, et al. Repair of large bone defects with the use of autologous bone marrow stromal cells. *N Engl J Med*. 2001;344(5):385-386.
9. Horwitz EM, Gordon PL, Koo WK, et al. Isolated allogeneic bone marrow-derived mesenchymal cells engraft and stimulate growth in children with osteogenesis imperfecta: implications for cell therapy of bone. *Proc Natl Acad Sci USA*. 2002;99(13):8932-8937.
10. Behnia H, Khojasteh A, Soleimani M, et al. Secondary repair of alveolar clefts using human mesenchymal stem cells. *Oral Surg Oral Med Oral Pathol Oral Radiol Endod*. 2009;108(2):e1-e6.
11. Marcacci M, Kon E, Moukhachev V, et al. Stem cells associated with macroporous bioceramics for long bone repair: 6- to 7-year outcome of a pilot clinical study. *Tissue Eng*. 2007;13(5):947-955.
12. Posel C, Moller K, Frohlich W, Schulz I, Boltze J, Wagner DC. Density gradient centrifugation compromises bone marrow mononuclear cell yield. *PLoS One*. 2012;7(12):e50293.
13. Korf-Klingebiel M, Kempf T, Sauer T, et al. Bone marrow cells are a rich source of growth factors and cytokines: implications for cell therapy trials after myocardial infarction. *Eur Heart J*. 2008;29(23):2851-2858.
14. Hisatome T, Yasunaga Y, Yanada S, Tabata Y, Ikada Y, Ochi M. Neovascularization and bone regeneration by implantation of autologous bone marrow mononuclear cells. *Biomaterials*. 2005;26(22):4550-4556.
15. Du F, Wu H, Li H, et al. Bone marrow mononuclear cells combined with beta-tricalcium phosphate granules for alveolar cleft repair: a 12-month clinical study. *Sci Rep*. 2017;7(1):13773.
16. Xiao X, Wang W, Liu D, et al. The promotion of angiogenesis induced by three-dimensional porous beta-tricalcium phosphate scaffold with different interconnection sizes via activation of PI3K/Akt pathways. *Sci Rep*. 2015;5:9409.
17. Centeno C, Pitts J, Al-Sayegh H, Freeman M. Efficacy of autologous bone marrow concentrate for knee osteoarthritis with and without adipose graft. *Biomed Res Int*. 2014;2014:370621.
18. Ramakrishnan A, Torok-Storb B, Pillai MM. Primary marrow-derived stromal cells: isolation and manipulation. *Methods Mol Biol*. 2013;1035:75-101.
19. Wu H, Kang N, Wang Q, et al. The dose-effect relationship between the seeding quantity of human marrow mesenchymal stem cells and in vivo tissue-engineered bone yield. *Cell Transplant*. 2015;24(10):1957-1968.
20. Rider KA, Flick LM. Differentiation of bone and soft tissues in formalin-fixed, paraffin-embedded tissue by using methylene blue/acid fuchsin stain. *Anal Quant Cytol Histol*. 2004;26(5):246-248.
21. Goldner J. A modification of the masson trichrome technique for routine laboratory purposes. *Am J Pathol*. 1938;14(2):237-243.
22. Mansfield JC, Winlove CP, Moger J, Matcher SJ. Collagen fiber arrangement in normal and diseased cartilage studied by polarization sensitive nonlinear microscopy. *J Biomed Opt*. 2008;13(4):044020.
23. Rice WL, Firdous S, Gupta S, et al. Non-invasive characterization of structure and morphology of silk fibroin biomaterials using non-linear microscopy. *Biomaterials*. 2008;29(13):2015-2024.
24. Uckermann O, Galli R, Beiermeister R, et al. Endogenous two-photon excited fluorescence provides label-free visualization of the inflammatory response in the rodent spinal cord. *Biomed Res Int*. 2015;2015:859084.
25. Mansfield JC, Winlove CP. A multi-modal multiphoton investigation of microstructure in the deep zone and calcified cartilage. *J Anat*. 2012;220(4):405-416.
26. Monici M. Cell and tissue autofluorescence research and diagnostic applications. *Biotechnol Annu Rev*. 2005;11:227-256.
27. de Souza RA, Xavier M, Mangueira NM, et al. Raman spectroscopy detection of molecular changes associated with two experimental models of osteoarthritis in rats. *Lasers Med Sci*. 2014;29(2):797-804.
28. Gamsjaeger S, Hofstetter B, Fratzl-Zelman N, et al. Pediatric reference Raman data for material characteristics of iliac trabecular bone. *Bone*. 2014;69:89-97.
29. Yerramshetty JS, Lind C, Akkus O. The compositional and physicochemical homogeneity of male femoral cortex increases after the sixth decade. *Bone*. 2006;39(6):1236-1243.
30. Morris MD, Mandair GS. Raman assessment of bone quality. *Clin Orthop Relat Res*. 2011;469(8):2160-2169.
31. McCreadie BR, Morris MD, Chen TC, et al. Bone tissue compositional differences in women with and without osteoporotic fracture. *Bone*. 2006;39(6):1190-1195.
32. de Souza RA, Xavier M, da Silva FF, et al. Influence of creatine supplementation on bone quality in the ovariectomized rat model: an FT-Raman spectroscopy study. *Lasers Med Sci*. 2012;27(2):487-495.

33. Oliver WC, Pharr GM. An improved technique for determining hardness and elastic modulus using load and displacement sensing indentation experiments. *J Mater Res*. 1992;7(06):1564-1583.
34. Yang CY, Simmons DJ, Lozano R. The healing of grafts combining freeze-dried and demineralized allogeneic bone in rabbits. *Clin Orthop Relat Res*. 1994;(298):286-295.
35. Kretlow JD, Jin YQ, Liu W, et al. Donor age and cell passage affects differentiation potential of murine bone marrow-derived stem cells. *BMC Cell Biol*. 2008;9:60.
36. Li C, Wei G, Gu Q, et al. Donor age and cell passage affect osteogenic ability of rat bone marrow mesenchymal stem cells. *Cell Biochem Biophys*. 2015;72(2):543-549.
37. Ikumi A, Funayama T, Tsukanishi T, Noguchi H, Yamazaki M. Novel unidirectional porous beta-Tricalcium phosphate used as a bone substitute after excision of benign bone tumors of the hand: a case series. *J Hand Surg Asian Pac Vol*. 2018;23(3):424-429.
38. LeGeros RZ. Properties of osteoconductive biomaterials: calcium phosphates. *Clin Orthop Relat Res*. 2002;395:81-98.
39. Chou J, Hao J, Kuroda S, Ben-Nissan B, Milthopre B, Otsuka M. Bone regeneration of calvarial defect using marine calcareous-derived beta-tricalcium phosphate macrospheres. *J Tissue Eng*. 2014;5:2041731414523441.
40. Bulgin D, Hodzic E. Autologous bone marrow-derived mononuclear cells combined with β-TCP for maxillary bone augmentation in implantation procedures. *J Craniofac Surg*. 2012;23(6):1728-1732.
41. Burket J, Gourion-Arsiquaud S, Havill LM, Baker SP, Boskey AL, van der Meulen MC. Microstructure and nanomechanical properties in osteons relate to tissue and animal age. *J Biomech*. 2011;44(2):277-284.
42. Soares LG, Marques AM, Guarda MG, et al. Raman spectroscopic study of the repair of surgical bone defects grafted or not with biphasic synthetic micro-granular HA + beta-calcium triphosphate irradiated or not with lambda 850 nm LED light. *Lasers Med Sci*. 2014;29(6):1927-1936.
43. Yin D, Wang Z, Gao Q, et al. Determination of the fate and contribution of ex vivo expanded human bone marrow stem and progenitor cells for bone formation by 2.3ColGFP. *Mol Ther*. 2009;17(11):1967-1978.
44. Kovtun A, Bergdolt S, Wiegner R, Radermacher P, Huber-Lang M, Ignatius A. The crucial role of neutrophil granulocytes in bone fracture healing. *Eur Cell Mater*. 2016;32:152-162.
45. Strohschein K, Radojewski P, Winkler T, Duda GN, Perka C, von Roth P. In vivo bioluminescence imaging - a suitable method to track mesenchymal stromal cells in a skeletal muscle trauma. *Open Orthop J*. 2015;9:262-269.
46. Nakabayashi A, Kamei N, Sunagawa T, et al. In vivo bioluminescence imaging of magnetically targeted bone marrow-derived mesenchymal stem cells in skeletal muscle injury model. *J Orthop Res*. 2013;31(5):754-759.
47. Redaelli S, Bentivegna A, Foudah D, et al. From cytogenomic to epigenomic profiles: monitoring the biologic behavior of in vitro cultured human bone marrow mesenchymal stem cells. *Stem Cell Res Ther*. 2012;3(6):47.
48. Gharibi B, Hughes FJ. Effects of medium supplements on proliferation, differentiation potential, and in vitro expansion of mesenchymal stem cells. *Stem Cells Translational Medicine*. 2012;1(11):771-782.
49. Yoon DS, Lee KM, Kim SH, et al. Synergistic action of IL-8 and bone marrow concentrate on cartilage regeneration through upregulation of chondrogenic transcription factors. *Tissue Eng Part A*. 2016;22(3–4):363-374.
50. Shintani S, Murohara T, Ikeda H, et al. Augmentation of postnatal neovascularization with autologous bone marrow transplantation. *Circulation*. 2001;103(6):897-903.
51. Umemura T, Nishioka K, Igarashi A, et al. Autologous bone marrow mononuclear cell implantation induces angiogenesis and bone regeneration in a patient with compartment syndrome. *Circ J*. 2006;70(10):1362-1364.
52. Veronesi E, Murgia A, Caselli A, et al. Transportation conditions for prompt use of ex vivo expanded and freshly harvested clinical-grade bone marrow mesenchymal stromal/stem cells for bone regeneration. *Tissue Eng Part C Methods*. 2014;20(3):239-251.
53. Baba K, Yamazaki Y, Ikemoto S, Aoyagi K, Takeda A, Uchinuma E. Osteogenic potential of human umbilical cord-derived mesenchymal stromal cells cultured with umbilical cord blood-derived autoserum. *J Craniomaxillofac Surg*. 2012;40(8):768-772.
54. Cassano JM, Kennedy JG, Ross KA, Fraser EJ, Goodale MB, Fortier LA. Bone marrow concentrate and platelet-rich plasma differ in cell distribution and interleukin 1 receptor antagonist protein concentration. *Knee Surg Sports Traumatol Arthrosc*. 2016;26:333-342.
55. Park MS, Kim YH, Jung Y, et al. In situ recruitment of human bone marrow-derived mesenchymal stem cells using chemokines for articular cartilage regeneration. *Cell Transplant*. 2015;24(6):1067-1083.
56. Takahashi T, Katsuta S, Tamura Y, et al. Bone-targeting endogenous secretory receptor for advanced glycation end products rescues rheumatoid arthritis. *Mol Med*. 2013;19:183-194.
57. Aikawa E, Fujita R, Asai M, Kaneda Y, Tamai K. Receptor for advanced glycation end products (RAGE)-mediated signaling impairs the maintenance of bone marrow mesenchymal stromal cells in diabetic model mice. *Stem Cells Dev*. 2016;25:1721-1732.
58. Czekanska EM, Ralphs JR, Alini M, Stoddart MJ. Enhancing inflammatory and chemotactic signals to regulate bone regeneration. *Eur Cell Mater*. 2014;28:320-334.

SUPPORTING INFORMATION

Additional supporting information may be found online in the Supporting Information section at the end of this article.

How to cite this article: Du F, Wang Q, Ouyang L, et al. Comparison of concentrated fresh mononuclear cells and cultured mesenchymal stem cells from bone marrow for bone regeneration. *STEM CELLS Transl Med*. 2021;10:598–609. https://doi.org/10.1002/sctm.20-0234